Solution Structures of the Antifungal Heliomicin and a Selected Variant with both Antibacterial and Antifungal Activities[†,‡]

Mireille Lamberty,[§] Anita Caille,[||] Céline Landon,[||] Séverine Tassin-Moindrot,[||] Charles Hetru,[§] Philippe Bulet,[§] and Françoise Vovelle*[,||]

Institut de Biologie Moléculaire et Cellulaire, Unité Propre de Recherche 9022, CNRS, "Réponse Immunitaire et Développement chez les Insectes", 15 rue René Descartes, 67084 Strasbourg Cedex, France, and Centre de Biophysique Moléculaire, Unité Propre de Recherche 4301, CNRS, affiliated with Orleans University, rue Charles-Sadron, 45071 Orléans Cedex 2, France

Received February 20, 2001; Revised Manuscript Received July 12, 2001

ABSTRACT: In response to an experimental infection, the lepidopteran *Heliothis virescens* produces an antifungal protein named heliomicin. Heliomicin displays sequence similarities with antifungal plant defensins and antibacterial or antifungal insect defensins. To gain information about the structural elements required for either antifungal or antibacterial activity, heliomicin and selected point-mutated variants were expressed in yeast as fusion proteins. The effects of mutations, defined by comparing the primary structure of heliomicin with the sequences of members of the insect defensin family, were analyzed using antibacterial and antifungal assays. One of the variants shows significant activity against Gram-positive bacteria while remaining efficient against fungi. The three-dimensional structures of this variant and of the wild-type protein were determined by two-dimensional ^{1}H NMR to establish a correlation between structure and antibacterial or antifungal activity. Wild-type and mutated heliomicins adopt a similar scaffold, including the so-called cysteine-stabilized $\alpha\beta$ motif. A comparison of their structures with other defensin-type molecules indicates that common hydrophobic characteristics can be assigned to all the antifungal proteins. A comparative analysis of various structural features of heliomicin mutant and of antibacterial defensins enables common properties to be assessed, which will help to design new mutants with increased antibacterial activity.

It has become clear that antimicrobial proteins are a key element of the immune response in multicellular organisms in protecting themselves against infectious microorganisms (*1*). Many of these proteins possess a broad spectrum of antimicrobial activity affecting bacteria and/or fungi, viruses, or parasites (*2*−*4*). Among these antimicrobial peptides, cysteine-rich molecules are the most widespread. They are found in plants, invertebrates, and vertebrates (*5*). Insect defensins are a group of cysteine-rich proteins mainly active against Gram-positive bacteria and occasionally against Gram-negative strains and filamentous fungi. They have been found in all insect species investigated so far. Recently, a cysteine-rich protein whose primary structure exhibits similarities to insect defensins has been isolated from the noctuidan *Heliothis virescens* (*6*). This molecule, named heliomicin, is inactive against bacteria but has a potent antifungal activity. Heliomicin also displays sequence similarities with drosomycin, an inducible antifungal protein isolated from *Drosophila melanogaster* (*7*). Both molecules are active against a large number of fungi at rather low concentrations (<2 μM). In contrast to drosomycin, which is inactive against yeast, heliomicin is active against two yeast strains, *Candida albicans* and *Cryptococcus neoformans* (*6*). In addition, the activity of heliomicin is retained at physiological ionic strength (137 mM NaCl), whereas a drop in drosomycin activity is observed.

Insect defensins are cysteine-rich cationic proteins with a molecular mass of ∼4 kDa (*5*). Comparison of the primary structures of a series of insect defensins, drosomycin and heliomicin, reveals the existence of a consensus motif of six cysteines forming three disulfide bridges. As already observed in plant defensins, drosomycin has an additional disulfide bridge between its N- and C-termini. The three-dimensional (3D) structures of *Phormia terranovae* defensin A and drosomycin have been determined by two-dimensional (2D) ^{1}H NMR spectroscopy in aqueous solution (*8*, *9*). The global fold of the two proteins includes a cysteine-stabilized $\alpha\beta$ motif (CS$\alpha\beta$ motif) (*8*) consisting of an α-helix and a two- or three-stranded β-sheet for the insect defensin or drosomycin, respectively. In this motif, the two cysteine residues located one turn apart in the α-helix form two disulfide bridges to two cysteine residues separated by a single amino acid in the last strand of the β-sheet (Cys-Xaa$_3$-Cys of the α-helix linked to the Cys-Xaa-Cys sequence of the β-sheet). The CS$\alpha\beta$ fold of insect defensins, initially

[†] This work was supported in part by the Centre National de la Recherche Scientifique and the Fondation pour la Recherche Médicale.

[‡] The sequence of heliomicin has been deposited in the Swiss-Prot Data Bank with accession code P81544. Heliomicin is a patented molecule (Patent PCT/FR99/00843. The coordinates of heliomicin Hel-Wt and of its mutant Hel-LL were deposited in the Protein Data Bank as entries 1I2U and 1I2V, respectively.

* To whom correspondence should be addressed. Telephone: +33238255574. Fax: +33238631517. E-mail: vovelle@cnrs-orleans.fr.

[§] Unité Propre de Recherche 9022, CNRS.

[||] Unité Propre de Recherche 4301, CNRS.

10.1021/bi0103563 CCC: $20.00
Published on Web 09/11/2001

identified in scorpion toxins (*10*, *11*), was also found in plant defense proteins (*12*−*14*) and in brazzein, a sweet-tasting protein (*15*).

In an attempt to understand the structural features required for the antifungal activity in heliomicin versus the antibacterial properties of insect defensins, the establishment of the 3D structure of heliomicin was required. In this study, we present the solution structure of the yeast-expressed heliomicin, determined by NMR spectroscopy and restrained molecular dynamics. The comparison of the solution structure of heliomicin with the structures of (1) antifungal drosomycin, (2) the plant defense antifungal protein *Raphanus sativus* protein 1 (*Rs*-AFP1), and (3) the antibacterial *P. terranovae* defensin A provides insight into the structure−function relationship of this class of antimicrobial proteins. In addition, site-directed mutagenesis was performed on heliomicin on the basis of primary structure alignments with insect defensins, enabling a mutated protein (Hel-LL) to be selected with a gain in antibacterial activity compared to the wild-type heliomicin (Hel-Wt). The solution structure of Hel-LL, where the amino acids Lys23 and Arg24 were replaced with two leucines, has been determined by 2D ^{1}H NMR spectroscopy and compared to the 3D structure of Hel-Wt and *Phormia* defensin A.

EXPERIMENTAL PROCEDURES

Synthetic Gene Construction. The yeast *Saccharomyces cerevisiae* strain TGY 48-1 was used for the production of wild-type heliomicin (Hel-Wt) and the mutant proteins. Expression was performed as described previously (*6*). Mutated heliomicins were prepared by replacing some of the oligonucleotides (SEA-5 to SEA-10) (*6*) of the native molecule with specific nucleotides to introduce the mutation sites. The following heliomicins with one mutation site were prepared: (i) heliomicin AAAA (Hel-AAAA), replacement of the N-terminal tetrapeptide Asp1-Lys2-Leu3-Ile4 of the native protein with four alanine residues; (ii) heliomicin A19-A20 (Hel-AA), substitution of residues Asn19 and Gly20 with two alanine residues; (iii) heliomicin L23-L24 (Hel-LL), replacement of the basic amino acids Lys23 and Arg24 with two hydrophobic leucine residues; and (iv) heliomicin R43 (Hel-R), substitution of the acidic amino acid Glu43 with a basic amino acid (Arg43). Using the sites for the restriction enzyme incorporated into the synthetic gene, the two, three, and four mutation sites were constructed and expressed in *S. cerevisiae*. For heliomicin A19A20L23L24 (Hel-AALL), two oligonucleotides were required to overcome the absence of a restriction site between the sequence encoding amino acids Asn19 and Gly20 and the sequence encoding residues Lys23 and Arg24 of heliomicin.

Purification, Integrity, and Purity Control of the Recombinant Proteins. Cloning procedures, yeast cell transformations, and protein purification were performed as previously described (*6*). However, the second step of purification by HPLC was replaced with solid-phase extraction onto Sep-Pak CM cartridges (Waters). The recombinant heliomicins, eluted with 1 M NaCl prepared in ammonium acetate buffer (25 mM at pH 3.6), were further purified by RP-HPLC[1] using a linear biphasic gradient of acetonitrile adapted to each protein. Finally, the proteins were lyophilized and kept as dry powder. Purity was ascertained by capillary zone electrophoresis (CZE) (270-A-HT, Applied Biosystems) under conditions previously described (*6*). Mass measurements were performed on a Bruker (Bremen, Germany) Biflex III MALDI-TOF mass spectrometer in a positive linear mode. An external calibration was performed using standard *Drosophila* antimicrobial peptides (drosocin, metchnikowin, and drosomycin at $[M + H]^+$ values of 2199.5, 3046.4, and 4890.5, respectively).

Antimicrobial Assays. The following fungal strains (gifts from W. Broekaert, Leuven, Belgium) were used: *Neurospora crassa* (CBS 327-54), *Fusarium culmorum* (IMI 180420), and *Nectria haematococca* (Collection Van Etten 160-2-2). Antibacterial assays were performed against *Micrococcus luteus* A270 (Pasteur Institute, Paris, France), *Bacillus megaterium* from J. Millet and A. Klier (Pasteur Institute), and *Escherichia coli* D22 from P. Boquet (CEA, France). Determination of minimal inhibitory concentrations (MICs) was carried out by liquid growth inhibition assays under previously described conditions (*16*). MICs are expressed as the [a]−[b] interval of concentrations, where [a] is the highest concentration tested at which the microorganisms are growing and [b] is the lowest concentration that causes 100% growth inhibition (*17*).

Nuclear Magnetic Resonance. NMR experiments were performed on 4 mM solutions prepared in sodium acetate buffer at pH 4.3. ^{1}H DQF-COSY, TQF-COSY (*18*), TOCSY (*19*, *20*), and NOESY (*21*) spectra were recorded at 293 K on a Bruker AMX-500 spectrometer equipped with three axis gradient coils. The water signal was suppressed using the WATERGATE pulse sequence (*22*). The exchange kinetics of amide protons were estimated from 1D (one-dimensional) and 2D spectra recorded at 293 K, after dissolution of the lyophilized sample in D_2O. All NMR data sets were processed on a Bruker X32 workstation and analyzed with XEASY software (*23*).

Structure Calculations. Starting from 200 random conformations, we determined the 3D solution structures by repeated rounds of DYANA calculation (*24*). From the 120 ms NOESY spectra were deduced interproton distances using the CALIBA program (*25*) and $^3J_{HN-H\alpha}$ coupling constants using INFIT (*26*). Programs included in the DYANA package allow definition of constraints for the ϕ, ψ, and χ^1 dihedral angles and stereospecific assignments with HABAS (*27*) and GLOMSA (*25*) and incorporation of additional restraints using NOAH (*24*). The final NMR restraint set included for heliomicin 130 intraresidue, 163 sequential, 105 medium-range, and 198 long-range restraints deduced from NOEs and 85 dihedral restraints. These values were 120, 172, 108, 190, and 100, respectively, for the mutant. Nine distance restraints corresponding to the three disulfide bridges were added for each molecule, and 14 hydrogen bonds (13 for the mutant), detected by DYANA and in agreement with the amide exchange data, were added during further steps of the refinement. Forty DYANA structures with target

[1] Abbreviations: RP-HPLC, reversed-phase high-performance liquid chromatography; CZE, capillary zone electrophoresis; MALDI-TOF, matrix-assisted laser desorption ionization time-of-flight; MS, mass spectrometry; MIC, minimal inhibitory concentration; DQF-COSY, double-quantum-filtered correlation spectroscopy; TOCSY, total correlation spectroscopy; NOESY, nuclear Overhauser enhancement spectroscopy; TQF-COSY, triple-quantum-filtered correlation spectroscopy.

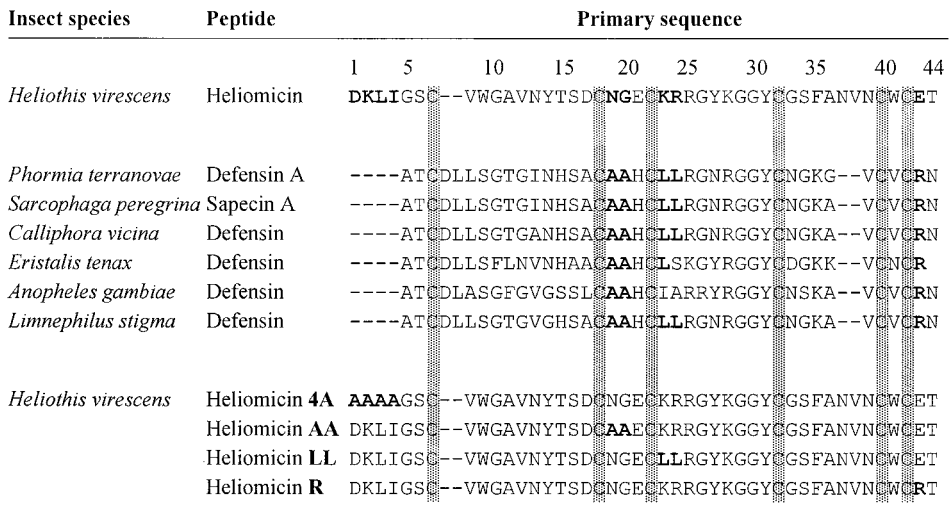

FIGURE 1: Comparison of the sequence of heliomicin from *H. virescens* with some insect defensins, and selection of mutation sites. The peptides are listed under the source organism. Residues conserved among the insect antibacterial defensins (bold) but subject to charge or polarity differences in heliomicin were selected for site specific mutagenesis. Homologous cysteine residues are boxed. The resulting mutated peptides expressed in *S. cerevisiae* were named heliomicin AAAA (Hel-AAAA, replacement of the four N-terminal residues with four Ala residues), heliomicin AA (Hel-AA, substitution of the Asn19-Gly20 dipeptide with two Ala residues), heliomicin LL (Hel-LL, replacement of the Lys23-Arg24 dipeptide with two Leu residues), and heliomicin R (Hel-R, substitution of Glu43 with Arg). In the same way, molecules mutated two, three, and four times were expressed.

Table 1: Production Rate and Antimicrobial Activity Spectrum of the Heliomicin Analogues Compared to Those of Wild-Type Heliomicin from *H. virescens*[a]

heliomicin	production rate (mg/L)	fungal strain			bacterial strain		
		N. crassa	*F. culmorum*	*N. haematococca*	*M. luteus*	*B. megaterium*	*E. coli*
wild-type	2.50	0.1−0.2	0.2−0.4	0.4−0.8	ND	ND	ND
AAAA	0.34	1.5−3	3−6	6−12	12−25	25−50	ND
AA	0.82	0.1−0.2	0.2−0.4	0.4−0.8	ND	ND	ND
LL	0.83	0.2−0.4	0.4−0.8	0.8−1.5	12−25	25−50	ND
R	0.47	0.1−0.2	0.2−0.4	0.4−0.8	50−100	50−100	ND
AAAA/R	0.30	1.5−3	3−6	6−12	50−100	50−100	ND
AAAA/AA	0.38	1.5−3	3−6	6−12	25−50	ND	ND
AAAA/LL	0.11	ND	ND	ND	12−25	25−50	ND
AA/R	0.86	0.1−0.2	0.2−0.4	0.4−0.8	25−50	50−100	ND
LL/R	0.44	0.2−0.4	0.4−0.8	0.8−1.5	ND	ND	ND
AA/LL	0.25	0.2−0.4	0.4−0.8	0.8−1.5	ND	ND	ND
AAAA/AA/R	0.52	1.5−3	3−6	6−12	50−100	50−100	ND
AAAA/LL/R	0.39	ND	ND	ND	ND	ND	ND
AAAA/AA/LL	0.15	ND	ND	ND	ND	ND	ND
AA/LL/R	0.27	0.2−0.4	0.4−0.8	0.8−1.5	ND	ND	ND
AAAA/AA/LL/R	0.14	ND	ND	ND	ND	ND	ND

[a] The heliomicin analogues are named according to the mutated sites on the peptide. The production rate is reported in milligrams of pure compound per liter of culture medium. The MIC is expressed in micromolar as a final concentration. Several peptide dilutions (50−0.1 μM for the antifungal assays and 100−0.2 μM for the antibacterial assays) were tested in liquid growth inhibition assays using three fungal and bacterial strains for MIC determination. The MIC has the definition proposed by Casteels and co-workers (*17*). ND means that no activity was detected at the highest concentration that was tested (50 μM for the antifungal and 100 μM for the antibacterial tests).

functions <2 Å^2 were energy minimized with the CHARMM force field (*28*) implemented in X-PLOR software (*29*). Two sets of 18 structures showing the lowest number of residual violations on distance restraints (<0.2 Å) were considered as representative of the solution structure of Hel-Wt and Hel-LL and were used for further analysis with PROCHECK (*30*, *31*) and PROMOTIF (*32*).

RESULTS

Expression and Purification of Recombinant Hel-Wt. To produce a sufficient amount of native heliomicin for detailed studies of its 3D structure, 10 mg of recombinant wild-type heliomicin (Hel-Wt) was expressed in yeast. The fusion protein carries at its N-terminus the prepro sequence derived from the precursor of the yeast pheromone-mating factor α1. This sequence allows secretion of the biologically active protein in a correctly processed form. Hel-Wt was subsequently purified according to the procedure described in Experimental Procedures. The integrity (including the presence of three disulfide bridges) and purity of the recombinant compound were confirmed by CZE and MALDI-TOF mass spectrometry using heliomicin (native) isolated from *H. virescens* larvae as an internal reference (data not shown). The mass measured at $[M + H]^+$ (4785.6) is in perfect agreement with the mass measured for native heliomicin (4785.8, MH^+) and its theoretical calculated average mass (4785.3, MH^+).

Selection, Expression, and Purification of Heliomicin Analogues. Heliomicin shows sequence similarities to antibacterial insect defensins (Figure 1), including the conserved

Table 2: Structural Statistics of the 18 Selected Structures of Heliomicin Solution Structure and of the 18 Structures of the LL Mutant

	Hel-WT		Hel-LL	
average no. of violations of experimental restraints	mean	min, max	mean	min, max
distance violations >0.3 Å	0.0	0, 0	0.02	0, 1
distance violations >0.2 Å	1.4	0, 3	1.2	0, 2
dihedral angle violations >10°	0.7	0, 2	0.0	0, 0

	Hel-WT		Hel-LL	
no. of deviations from idealized geometry	mean	min, max	mean	min, max
bond distances >0.05 Å	2.7	0, 4	2.3	0, 4
angles >10°	0.7	0, 2	0.6	0, 2

	Hel-WT	Hel-LL
Ramachandran maps (%)[a]	mean	mean
most favorable regions	61	60
additional regions	31	34

	Hel-WT		Hel-LL	
rmsd (Å)	paiwise	mean structure	pairwise	mean structure
all backbone atoms (N, Cα, and C)	0.56 ± 0.12	0.38 ± 0.05	0.94 ± 0.22	0.82 ± 0.29
secondary structures (N, Cα, and C)[b]	0.34 ± 0.10	0.29 ± 0.10	0.41 ± 0.13	0.37 ± 0.12
all atoms	1.61 ± 0.14	1.10 ± 0.09	1.89 ± 0.29	1.49 ± 0.44

energy (kcal/mol)[c]	Hel-WT	Hel-LL
E (electrostatic)	−652 ± 18	−666 ± 29
E (van der Waals)	−153 ± 6	−156 ± 8
E (NOE)	14.4 ± 2.2	10.3 ± 1.2

[a] Ramachandran plots were calculated with PROCHECK. [b] The secondary structure elements are defined by residues 2−6, 17−25, 30−32, and 39−42. [c] The energy terms were calculated using the CHARMM 19 force field implemented in X-PLOR with a distance-dependent dielectric function and a cutoff distance of 12 Å for all nonbonded interactions. The NOE energy terms were calculated with a force constant of 50 kcal mol^{-1} $Å^{-2}$ for distance restraints and 1 kcal mol^{-1} rad^{-2} for angular restraints.

array of cysteines. On the basis of sequence alignment with insect defensins, different heliomicin analogues were expressed in *S. cerevisiae* to confer antibacterial activity to these proteins. Amino acids conserved among the insect antibacterial defensins but subject to charge differences in the antifungal heliomicin were considered to be suitable candidate residues for site-specific mutational analysis. Four series of heliomicin variants were generated (Figure 1). (i) In Hel-AA, the hydrophilic residues Asn19 and Gly20 were replaced with two alanines (Ala19 and Ala20) as found in most insect defensins. (ii) In the variant Hel-LL, the Leu23-Leu24 dipeptide is substituted for the Lys23-Arg24 sequence, since the antibacterial defensins, except those of *Eristalis tenax* and *Anopheles gambiae* (*5*), have leucines at these two positions. (iii) A basic residue (Arg) is conserved in the C-terminal part of the defensin sequences, while heliomicin has an acidic residue (Glu43) at this position. In Hel-R, Glu43 is mutated to Arg43. (iv) The last mutation site concerns the four-residue N-terminal extension absent in antibacterial defensins. In the fourth series of variants, the N-terminal tetrapeptide Asp-Lys-Leu-Ile was replaced with a four-alanine peptide (Hel-AAAA).

Yeast expression, production, and purification of the heliomicin variants were performed essentially as described for Hel-Wt (*6*). After final purification, the integrity and purity of recombinant proteins were controlled according to the procedure used for Hel-Wt. The molecular mass of each compound measured by MALDI-TOF-MS was in agreement with the values predicted using the ProMaC 1.5.3 program (data not shown). The variation between the molecular masses measured and the calculated molecular masses did not exceed 1.4 Da (obtained for Hel-LLR). The overall yield of pure protein varies from 0.11 to 0.86 mg/L of culture medium depending upon the isoform that is considered (Table 1).

Activity Study of Heliomicin Analogues on Microorganisms. As only limited quantities of pure proteins were obtained for different mutated proteins (Hel-AAAAR and Hel-AAAA), only six microorganisms were selected for assessment of their antimicrobial properties. The fungi *N. crassa*, *F. culmorum*, and *N. haematococca* were selected as Hel-Wt revealed the strongest activity against these fungal strains (*6*). In addition, heliomicin variants were tested against the Gram-positive *M. luteus* and *B. megaterium* and the Gram-negative *E. coli* D22, in general the strains most sensitive to insect defensins. The results that were obtained are reported in Table 1. The largest decrease in antifungal activity was observed for all the heliomicin analogues containing four-alanine replacements. Replacement of the Asp-Lys-Leu-Ile sequence with four alanine residues results in a 15-fold decrease in antifungal potency against the three fungal strains tested compared to Hel-Wt. The Hel-LL variants, carrying hydrophobic amino acids instead of basic residues, showed a 2-fold reduction in antifungal activity compared to Hel-Wt. Hel-AAAA/LL, with two mutation sites, is inactive on *N. crassa*, *F. culmorum*, and *N. haematococca* at the highest concentration that was tested (50 μM). The same pattern of results was obtained for the proteins with three and four mutation sites exhibiting the N-terminal substitution and the hydrophobic Leu-Leu replacements. No difference in antifungal activity was observed for Hel-AA and Hel-R (Table 1). The minimal inhibitory

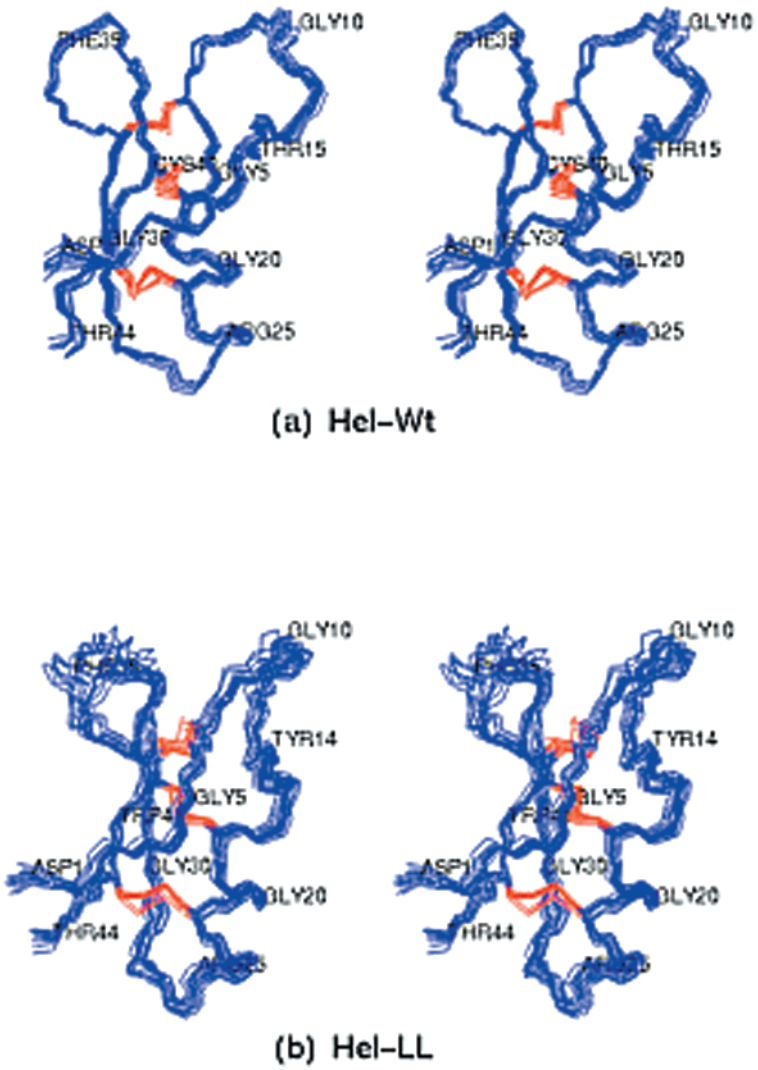

FIGURE 2: Stereoscopic viewes of a best fit superposition of the α-carbons of the 15 solution structures of heliomicin wild-type Hel-Wt (a) and Hel-LL (b).

concentrations (MICs; *17*) on the three fungal strains were identical to that observed for the wild-type protein. Similarly, Hel-AA/R did not show any decrease in antifungal activity compared to the native molecule. Furthermore, the presence of the Ala19-Ala20 and/or Arg43 mutation(s) in heliomicin had no additional effect on the decrease of antifungal potency observed for Hel-AAAA and Hel-LL. In fact, the antifungal activities of Hel-AAAA/R, -AAAA/AA, and -AAAA/AA/R were comparable to the activity of the AAAA analogue. Hel-LL/R, -AA/LL, and -AA/LL/R exhibited antifungal properties similar to those of Hel-LL (Table 1).

Measurement of the effect of heliomicin analogues on *E. coli* D22 did not reveal any activity even at concentrations up to 100 μM. However, the single mutation sites AAAA, LL, and R in heliomicin conferred antibacterial activity against both Gram-positive strains tested (*M. luteus* and *B. megaterium*) (Table 1). Hel-AAAA and Hel-LL were active against *M. luteus* and *B. megaterium* at MICs of 12−25 and 25−50 μM, respectively, while Hel-R exhibited moderate activity against these strains (MIC = 50−100 μM). Hel-AA, even at 100 μM, was inactive against the three bacterial strains that were tested. Some of the mutated heliomicin proteins carrying two mutation sites were also active against the Gram-positive strains. Hel-AAAA/R, -AAAA/AA, -AAAA/LL, and -AA/R exhibited significant antibacterial activity against *M. luteus* and *B. megaterium* (Table 1). Hel-LL/R and -AA/LL with two mutation sites did not exhibit antibacterial activity. Among the heliomicin molecules with three mutation sites, only Hel-AAAA/AA/R was found to affect the growth of the two Gram-positive bacteria. Surprisingly, Hel-AAAA/AA/LL/R (four mutation sites) was inactive on bacteria, although its primary structure is the closest to that of insect defensins.

Among the mutated proteins, only Hel-LL exhibited significant anti-Gram-positive activity without a large reduction in antifungal activity compared to Hel-Wt (only 2-fold). Therefore, in an attempt to evaluate the structural features responsible for this difference in activity, the 3D structure of the mutant Hel-LL was determined.

Structural Features. All proton resonances of Hel-Wt and of Hel-LL were defined using the standard sequence specific assignment strategy (*33*) from the ^{1}H DQF-COSY, TOCSY, and NOESY spectra. For the two proteins, an examination of the NOE data, ^3J coupling constants, and hydrogen exchange rates for HN protons provided evidence for three strands of β-sheet and an α-helical region. The 3D structures of both proteins were determined according to the procedure described in Experimental Procedures. The structural statis-

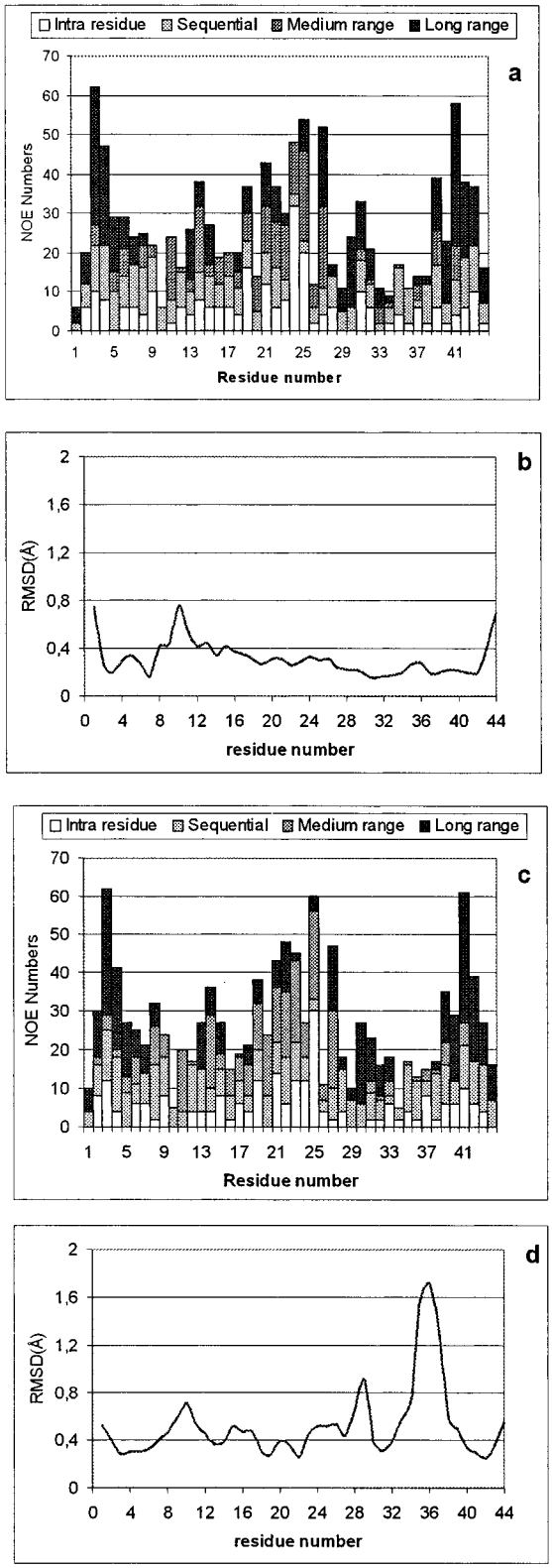

FIGURE 3: (a) Number of NOEs per residue for Hel-Wt: intraresidue (white), sequential (light gray), medium-range (dark gray), and long-range (black). (b) Local rmsd, for Hel-Wt, calculated for the N, Cα, and C atoms with respect to the average structure. (c) Number of NOEs per residue for Hel-LL. (d) Local rmsd for Hel-LL.

tics (Table 2) and a superposition of the selected structures (Figure 2) revealed their good definition. This is particularly evident in the region of regular secondary structure elements, where the average pairwise rms deviations of the coordinates of the backbone atoms are 0.34 ± 0.10 and 0.41 ± 0.13 Å for Hel-Wt and Hel-LL, respectively. In addition, the structures are in good agreement with the experimental data since, on average, only 1.4 and 1.2 distance violations larger than 0.2 Å per structure were observed for Hel-Wt and Hel-LL, respectively.

Structure analysis, using PROCHECK (*30*, *31*) and PROMOTIF (*32*), reveals that the Hel-Wt global fold involves an α-helix from Asp17 to Arg25 and a three-stranded antiparallel β-sheet, including residues 2−6 for the first strand, 30−32 for the second, and 39−42 for the last. The classical array of C═O (i)···NH ($i + 4$) hydrogen bonds is found in the helical part of the molecule. In the first strand of the β-sheet, a bulge at residues Ile4 and Gly5 leads to interruptions in the standard hydrogen bond network with the third strand. A long loop L1 (residues 7−16) connects the first strand of the β-sheet to the α-helix. The loop is stabilized by a γ-turn (residues 11−13) and backbone−backbone hydrogen bonds. A well-defined turn, T1, including residues 26−29, connects the α-helix to the second strand of the β-sheet, and the chain reversal is ensured by Gly26 which adopts a positive ϕ value. The second and third strands of the β-sheet are linked by a long turn, T2 (residues 33−38), including a type IV β-turn (residues 34−37). At the N-terminus of the α-helix, a hydrogen bond is observed between the Oδ of Asp17 and the NH group of Gly20 which was found to be slowly exchangeable in amide exchange experiments. This interaction can be classified as an N-capping interaction (*34*). Compared to the positions of aliphatic and other aromatic side chains, the position of Trp9 in loop L1 is poorly defined. There is a lack of precision in the definition of its side chains but also in the conformation of the backbone atoms: the angles of Val8 (ψ) and Trp9 (ϕ) adopt two different sets of values. Compared to Trp41, few NOE data are available for Trp9. Several Lys and Asn side chain positions are poorly defined, such as Asn13, Lys23, Asn37, and Asn39. However, they always point in the same direction, outward from the protein core.

The 3D structure of Hel-LL displays the same general features as Hel-Wt (Figure 2). The rms deviation of the backbone atoms of the minimized average structure between the two molecules is 1.35 Å. This value drops to 0.67 Å when calculated for the secondary structure elements (residues 2−6, 17−25, 30−32, and 39−42) and is as low as 0.45 Å for the helix, although this is where the mutation occurs. Very few structural changes appear at the site of mutation; the orientation of the Leu23 and Leu24 side chains is approximately identical to the orientation of Lys23 and Arg24 in Hel-Wt. Large differences between Hel-Wt and Hel-LL exist in loop L1 (residues 7−16). In both structures, a γ-turn stabilizes L1, between residues 8 and 10 in Hel-Wt and between residues 11 and 13 in Hel-LL. In heliomicin, turn T2 includes an additional β-turn between residues 33 and 36. The major difference between Hel-Wt and Hel-LL concerns the definition of the solution structures in loop L1 and turn T2 (Figure 2 and Table 2). The best fit superposition of the backbone atoms of loop L1 in the mutant shows that it is structurally well defined, with a rmsd of 0.42 ± 0.16 Å (0.52 ± 0.26 Å for Hel-Wt). However, it can adopt different orientations with respect to the rest of the molecule (Figure 2) as already observed in *Phormia* defensin A (*8*). Although the amount of NOE data in turn T2 of Hel-LL is not

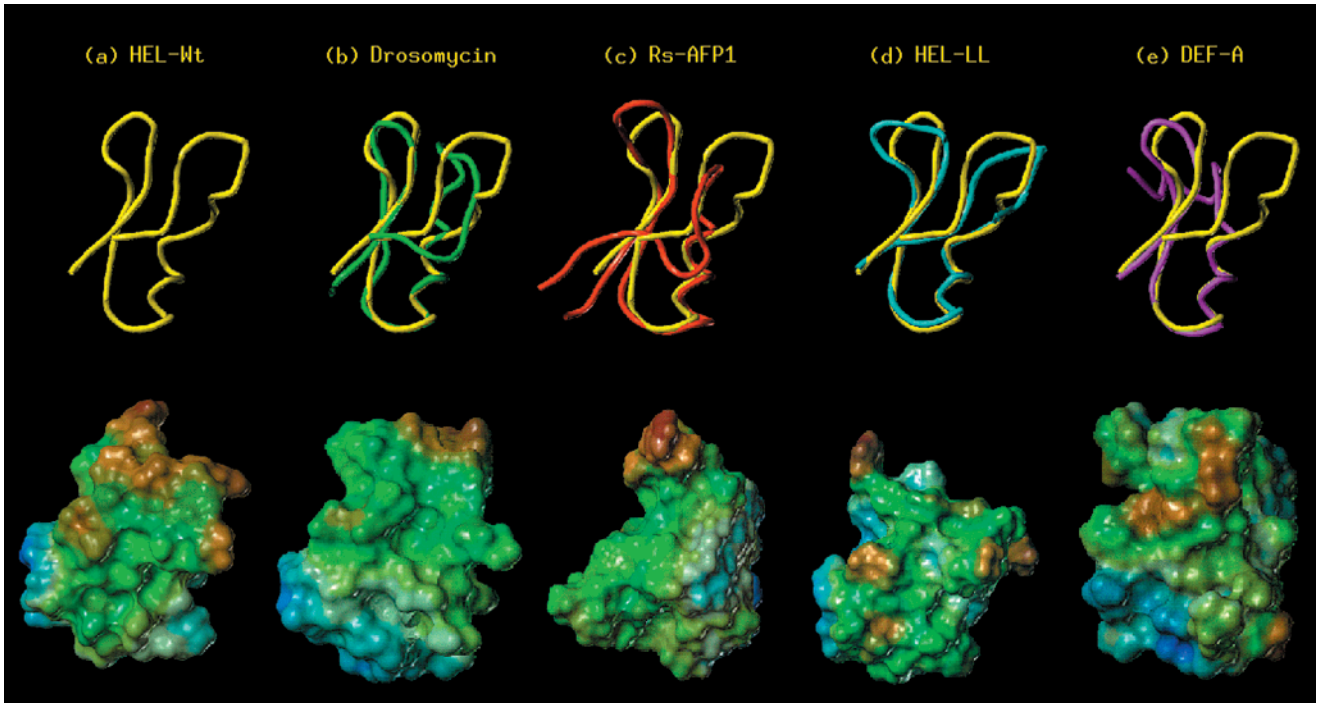

FIGURE 4: Best fit superposition of the global folds and lipophilic potential of (a) wild-type heliomicin, Hel-Wt (yellow), (b) drosomycin (green), (c) *Rs*-AFP1 (red), (d) heliomicin LL, Hel-LL (cyan), and (e) *Phormia* defensin A, Def-A (magenta). The best fit was obtained for the backbone heavy atoms corresponding to the common secondary structure elements. The lipophilic potentials are calculated with the MOLCAD option of SYBYL (*35*, *36*) on the Connoly surface of the molecules. Hydrophobic and hydrophilic surfaces are displayed in brown and blue, respectively, and green surfaces represent an intermediate hydrophobicity.

dramatically lower than in Hel-Wt (Figure 3a,c), the rmsd per residue (local rmsd) is large (Figure 3d). Conversely, in Hel-Wt, turn T2 adopts a well-defined conformation, with a very low local rmsd (Figure 3b).

DISCUSSION

Proteins with a CSαβ motif constitute a family of molecules with a large diversity of functions. This motif observed in antimicrobial proteins from plants (*12*) and invertebrates (*8*) has also been reported in neurotoxins (*10*, *11*) and in a sweet-tasting protein from fruit (*15*). This compact and well-organized scaffold, although not related to a common biological activity, confers to all these molecules a remarkable stability and a high resistance to proteases. The specificity of activity presumably results from the type of residues and from their arrangement on the scaffold formed by the CSαβ motif. Heliomicin is a member of this family showing an antifungal activity over a large spectrum of germs but is not active on bacteria (*6*). The global fold of heliomicin is characterized by the presence of a long loop, L1, connecting the first strand of the β-sheet to the α-helix and a long turn, T2, between the second and third strands of the sheet. Despite the presence of L1 and T2, all these structural elements are well-defined by the NOE data, leading to a compact and apparently rigid structure.

Heliomicin shares approximately 50% sequence similarity with drosomycin, a *D. melanogaster* antifungal defensin (*7*). Drosomycin is also active against a variety of fungal strains but not against *C. albicans*. The 3D structures adopted by drosomycin (*9*) and heliomicin in solution reveal a similar organization, a $\beta\alpha\beta\beta$ fold stabilized by a CSαβ motif. The rms deviation between the backbone atoms of the secondary structure elements of drosomycin and heliomicin is only 0.96 Å (Figure 4b). However, the first strand of the β-sheet involves five residues in heliomicin (2−6) and only three in drosomycin (2−4), while the second strand is shorter in heliomicin (30−32) than in drosomycin (30−34). In addition, the α-helix is two residues longer in drosomycin than in heliomicin (residues 16−26 and 17−25, respectively). But the main difference is observed in the conformations of loop L1 and turn T2. After best fitted superposition of the backbone atoms of residues 7−16 of heliomicin and drosomycin, the rms deviation between these atoms is large (4.1 Å). Hydrophobic interactions between strands I and III and between loop L1 and turn T2, supported by NOE connectivities between Leu3 and Trp41 protons and between Val8 and Val38 protons, maintain the compactness of the structure of heliomicin despite the absence of the additional disulfide bridge of drosomycin (Cys2−Cys44).

The antifungal plant defensin *Rs*-AFP1, from the radish *R. sativus* (*13*), which is only 28% similar to heliomicin, also adopts a CSαβ overall fold, including an α-helix and a three-stranded β-sheet, and the molecule is stabilized by four disulfide bridges. The rms deviation between the secondary structure elements of two selected structures of heliomicin and *Rs*-AFP1 is only 1.01 Å (1.02 Å between drosomycin and *Rs*-AFP1). A representation of the backbones of the two proteins (Figure 4c) indicates that, as already observed for drosomycin, the differences in the global fold of heliomicin and *Rs*-AFP1 are concentrated in loop L1 and turn T2.

In addition to similarities in their global folds, heliomicin, drosomycin, and *Rs*-AFP1 contain large clusters of hydrophobic residues. One cluster is formed by residues at the top of loop L1 and in turn T2 and a second one by residues located at the N- and C-termini. Both clusters are contiguous and form a large hydrophobic zone. An analysis of the

lipophilic potentials calculated on the Connolly surface of the molecules with MOLCAD (*35*, *36*) (Figure 4a−c) shows that, despite small differences in the distribution of potentials, the three molecules display an amphipathic character. The molecular face including the α-helix and the second strand of the *β*-sheet is hydrophilic. The other face (first and third strands of the *β*-sheet) is intermediate, while the head of the molecule (end of L1 and T2) is hydrophobic. The presence of such a hydrophobic area at the head of the molecule already reported for drosomycin and plant defense proteins (*37*) seems to be a feature common to three antifungal proteins.

Heliomicin and drosomycin have an overall identical total charge (+1), but the distributions of charges on the surface of the molecule are different, leading to distribution variations in electrostatic potentials (data not shown). Such differences could probably explain the difference in activity observed between drosomycin and heliomicin at high salt concentrations.

Although the level of sequence similarity is only 40%, heliomicin and *Phormia* defensin A display common structural features. A superposition of the Hel-Wt and defensin A global folds (Figure 4e) shows a very good fit of their CSα*β* motifs. The rms deviation of the backbone atoms of the motif is only 0.90 Å. However, the α-helix of heliomicin is three residues shorter than the α-helix of *Phormia* defensin A. In addition, large differences appear in the conformation of the N-terminal segment, since the first strand of the *β*-sheet is missing in *Phormia* defensin A, and in turn T2 which includes five residues in heliomicin and only three in *Phormia* defensin A.

Heliomicin is purely antifungal, while *Phormia* defensin A is preferentially active against Gram-positive bacteria. We have taken advantage of this observation to suggest the nature of the amino acids and their key position on the CSα*β* motif that conveys antibacterial versus antifungal activities. On the basis of sequence comparisons between antibacterial defensins and heliomicin, several site-directed mutations were introduced to confer antibacterial activity to heliomicin. Heliomicin was modified by four single-site mutations: three mutants (Hel-AAAA, Hel-LL, and Hel-R) acquired antibacterial activity, indicating the adequacy of the changes. Moreover, most proteins with two mutation sites exhibited significant antibacterial activity. Mutants with three and four mutation sites lost antibacterial activity but also lost antifungal activity (Table 1). This loss of function may be linked to alterations in the structure as a consequence of overly drastic modifications. It must be pointed out that all heliomicins are not produced at the same level in yeast (Table 1). This is probably related to misfolding or interactions with the yeast. Most antibacterial analogues retained strong antifungal activity, and the changes in the function of the molecule are more a widening of the activity spectrum than a real decrease in the activity on specific strains. Like *Phormia* defensin A, the antibacterial analogues are active only against Gram-positive bacteria and not against Gram-negative strains. This suggests that the amino acids introduced by mutagenesis in the antibacterial heliomicins may be responsible for their activity against Gram-positive bacteria. Among the various heliomicin variants that were studied showing a significant activity against Gram-positive bacteria, Hel-LL exhibits only a minor reduction in antifungal activity. For this reason, we have determined the 3D structure of the Hel-LL mutant.

The 3D structures of Hel-Wt and Hel-LL are very similar, except for small differences in the observed hydrogen bond network and a lower precision of the structure of the mutant in loop L1 and turn T2. In addition, in the mutant, loop L1 and turn T2 are much further apart so that the level of packing of the hydrophobic residues is reduced (Figure 4d). This leads to a decrease in the hydrophobicity of the head of the molecule, which may account for the slight reduction in antifungal activity of Hel-LL if one assumes the importance of the hydrophobic cluster for antifungal activity.

The substitution of the two basic residues, Lys23 and Arg24, at the end of the helix with two leucines gives rise to an amphiphilic character in the α-helix of Hel-LL. This amphiphilic character is a feature common to (i) the helices of all antibacterial insect defensins (for a review, see ref *5*) and (ii) some short helical antibacterial peptides such as cecropins (*38*) and magainins (*39*). In addition, this mutation modifies the repartition of hydrophobic potentials, leading to hydrophobic patches distributed all over the structure as observed on the *Phormia* defensin A surface (Figure 4a,d,e).

In conclusion, despite the absence of a fourth disulfide bridge, heliomicin, like the other purely antifungal defensins, drosomycin and *Rs*-AFP1, adopts a rigid *β*α*ββ* architecture, including the CSα*β* motif. These antifungal proteins exhibit very similar distributions of lipophilic potentials characterized by a hydrophobic region including residues of loop L1 and turn T2.

On the basis of sequence alignment with antibacterial defensins, we have designed a mutant (Hel-LL) of the antifungal heliomicin (Hel-Wt) that is active against Gram-positive bacteria. The comparison of several structure-related features of heliomicin, of its mutant, and of *Phormia* defensin A shows that the mutation tends toward a molecule that resembles *Phormia* defensin A more than heliomicin does. Obviously, the differences between Hel-Wt and Hel-LL are small, and Hel-LL is active against Gram-positive bacteria at a concentration higher than *Phormia* defensin A. Nevertheless, the Hel-LL mutant, as expected, is active against Gram-positive bacteria, and the information obtained for the 3D structure of heliomicin will allow the design of heliomicin analogues with increased antimicrobial potencies.

ACKNOWLEDGMENT

We thank Dr. Laurence Sabatier for mass spectrometry measurements and Martine Schneider for her technical assistance in the production of the recombinant heliomicin proteins.

SUPPORTING INFORMATION AVAILABLE

$^3J_{HN-\alpha H}$ values and chemical shifts of Hel-Wt and Hel-LL. This material is available free of charge via the Internet at http://pubs.acs.org.

REFERENCES

1. Ganz, T., and Lehrer, R. I. (1998) *Curr. Opin. Immunol. 10*, 41−44.
2. Boman, H. G. (1995) *Annu. Rev. Immunol. 13*, 61−65.
3. Hetru, C., Hoffmann, D., and Bulet, P. (1998) Antimicrobial peptides from insects, in *Molecular Mechanisms of Immune*

Response in Insects (Brey, P. T., and Hultmark, D., Eds.) pp 40−66, Chapman & Hall, London.
4. Bulet, P., Hetru, C., Dimarcq, J. L., and Hoffmann, D. (1999) *Dev. Comp. Immunol. 23*, 329−344.
5. Dimarcq, J. L., Bulet, P., Hetru, C., and Hoffmann, J. A. (1998) *Biopolymers 47*, 465−477.
6. Lamberty, M., Ades, S., Uttenweiler-Joseph, S., Brookhart, G., Bushey, D., Hoffmann, J. A., and Bulet, P. (1999) *J. Biol. Chem. 274*, 9320−9326.
7. Fehlbaum, P., Bulet, P., Michaut, L., Lagueux, M., Broekaert, W. F., Hetru, C., and Hoffmann, J. A. (1994) *J. Biol. Chem. 269*, 33159−33163.
8. Cornet, B., Bonmatin, J. M., Hetru, C., Hoffmann, J. A., Ptak, M., and Vovelle, F. (1995) *Structure 3*, 435−448.
9. Landon, C., Sodano, P., Hetru, C., Hoffmann, J. A., and Ptak, M. (1997) *Protein Sci. 6*, 1878−1884.
10. Bontems, F., Roumestand, C., Gilquin, B., Ménez, A., and Toma, F. (1991) *Science 254*, 1521−1523.
11. Possani, L., Becerril, B., Delepierre, M., and Tytgat, J. (1999) *Eur. J. Biochem. 264*, 287−300.
12. Bruix, M., Jiménez, M. A., Santoro, J., González, C., Colilla, F. J., Méndez, E., and Rico, M. (1993) *Biochemistry 32*, 715−724.
13. Fant, F., Vranken, W. F., Broeckaert, W., and Borremans, F. (1998) *J. Mol. Biol. 279*, 257−270.
14. Fant, F., Vranken, W. F., and Borremans, A. M. (1999) *Proteins 37*, 388−403.
15. Caldwell, J. E., Abildgaard, F., Dzakula, Z., Ming, D., Hellekant, G., and Markley, J. L. (1998) *Nat. Struct. Biol. 5*, 427−431.
16. Hetru, C., and Bulet, P. (1997) in *Methods in Molecular Biology* (Shafer, W. M., Ed.) Vol. 78, pp 35−49, Humana Press, Totowa, NJ.
17. Casteels, P., Ampe, C., Jacobs, F., and Tempst, P. (1993) *J. Biol. Chem. 268*, 7044−7054.
18. Piantini, U., Sørensen, O. W., and Ernst, R. R. (1982) *J. Am. Chem. Soc. 104*, 6800−6801.
19. Bax, A., and Davis, D. G. (1985) *J. Magn. Reson. 65*, 355−360.
20. Griesinger, C., Otting, G., Wüthrich, K., and Ernst, R. R. (1988) *J. Am. Chem. Soc. 110*, 7870−7872.
21. Jeener, J., Meier, B. H., Bachmann, P., and Ernst, R. R. (1979) *J. Chem. Phys. 71*, 4546−4553.
22. Piotto, M., Saudek, V., and Sklenar, V. (1992) *J. Biomol. NMR 2*, 661−665.
23. Bartels, C., Xia, T. E., Billeter, M., Güntert, P., and Wüthrich, K. (1995) *J. Biomol. NMR 5*, 1−10.
24. Güntert, P., Mumenthaler, C., and Wüthrich, K. (1997) *J. Mol. Biol. 273*, 283−298.
25. Güntert, P., Braun, W., and Wüthrich, K. (1991) *J. Mol. Biol. 217*, 517−530.
26. Szyperski, T., Güntert, P., Otting, G., and Wüthrich, K. (1992) *J. Magn. Reson. 99*, 552−560.
27. Güntert, P., and Wüthrich, K. (1991) *J. Biomol. NMR 1*, 447−456.
28. Brooks, B., Brucoli, R., Olafson, B. O., States, D. J., Swaminathan, S., and Karplus, M. (1983) *J. Comput. Chem. 4*, 187−217.
29. Brünger, A. T. (1992) *The X-PLOR software manual*, version 3.1, Yale University Press, New Haven, CT.
30. Laskowski, R. A. (1993) *J. Appl. Crystallogr. 26*, 283−291.
31. Laskowski, R. A., Rullmannn, J. A., MacArthur, M. W., Kaptein, R., and Thornton, J. M. (1996) *J. Biomol. NMR 8*, 477−486.
32. Hutchinson, E. G., and Thornton, J. M. (1996) *Protein Sci. 5*, 212−220.
33. Wüthrich, K. (1986) in *NMR of Proteins and Nucleic Acids* Wiley Interscience, New York.
34. Harper, E. W., and Rose, G. D. (1993) *Biochemistry 32*, 7605−7609.
35. Ghose, A. K., Pritchett, A., and Crippen, G. M. (1988) *J. Comput. Chem. 9*, 80−90.
36. Heiden, W., Moeckel, G., and Brickman, J. (1993) *J. Comput.-Aided Mol. Des. 7*, 503−514.
37. Landon, C., Pajon, A., Vovelle, F., and Sodano, P. (2000) *J. Pept. Res. 46*, 231−238.
38. Holak, T. A., Engström, A., Kraulis, P. J., Lindeberg, G., Bennich, H., Jones, T. A., Gronenborn, A. M., and Clore, G. M. (1988) *Biochemistry 27*, 207−217.
39. Gesell, J., Zasloff, M., and Opella, S. (1997) *J. Biomol. NMR 9*, 127−135.

BI0103563